


---

This is the **accepted version** of the journal article:

Parrón Granados, Josep; Cabrera-Hernández, Edith Annette; Tennant, Alan; [et al.]. «Multiport compact stacked patch antenna with 360° beam steering for generating dynamic directional modulation». IEEE Transactions on Antennas and Propagation, Vol. 69, Issue 2 (February 2021), p. 1162-1167. DOI 10.1109/tap.2020.3008065

---

This version is available at <https://ddd.uab.cat/record/273565>

under the terms of the  **IN** COPYRIGHT license

# Multiport Compact Stacked Patch Antenna with 360° beam steering for Generating Dynamic Directional Modulation

Josep Parron, Edith A. Cabrera-Hernandez, Alan Tennant and Pedro de Paco

**Abstract**— In this contribution, we propose a multiport compact antenna that supports four radiating modes operating at the same frequency thus making it a suitable candidate to substitute a linear array of four antennas. It will be also shown as this antenna produces dynamic directional modulation (DDM) with low bit error rate (BER) in a unique, unambiguous (secure) angular region that can be chosen freely in the XY plane. Trade-offs between the BER beam width of the secure angular region, the BER at side lobes and the extra power required in the generation of DDM are assessed through measurements with real-time data transmission.

**Index Terms**— Directional modulation (DM), multiport compact antenna, secure communication.

## I. INTRODUCTION

In recent years, directional modulation (DM) has been introduced as a transmission technique that can improve physical layer security of wireless communications [1]-[2]. DM uses different antenna radiation patterns to transmit a given constellation of symbols towards a desired secure observation angle while simultaneously transmitting distorted versions of the constellation to other observation angles [2].

Implementations of DM are often based on antenna arrays (dipoles, patches, etc.) excited with feeding networks that enable the configuration of different radiation patterns. Several DM beamforming techniques have been reported in the open literature including: switches [3]-[6], a dual-beam method [7], reconfigurable attenuators and/or phase shifters [8]-[10], vector modulators [11]-[14] and the use of a Fourier Rotman lens [15].

When the number of array elements antennas in a DM system is less than four, the spacing between elements is typically larger than  $\lambda$  (free space wavelength) [7], [11] and tends to  $\lambda/2$  as the number of elements in the array increases [5], [6], [8]-[10], [12]-[15]. In either case, the size of the resulting array is larger than several  $\lambda$ , which limits the use of DM to applications where the antenna size is not a constraint.

Another limitation of the many reported DM systems is the restricted angular range where the secure transmission can be achieved. For example, in a patch (directive antenna) array, the array factor is shaped by the patch radiation pattern, thus limiting the available angular range of secure transmit directions [5]-[9], [13], [15]. In contrast, if dipoles (omnidirectional antennas) are used [10]-[12], [14], the symmetry of the array generates a symmetric H plane radiation pattern resulting in two angular directions transmitting the same information in both the forward and rear hemispheres.

Recently, a multiport compact antenna with maximum dimensions of the order of  $\lambda/2$  was presented for generating DM with 360° beam steering [16]. The full circular angular coverage was achieved

through the combination of the radiation patterns of a monopole and a circular patch with two orthogonal  $TM_{21}$  modes excited simultaneously in quadrature [17]. This configuration allows for the introduction of phase variation without the need for spacing between array elements. However, the combination of these two radiation patterns produces a wide beam width and a reduced bit error rate (BER) not only in the desired secure direction, but also in the opposing hemisphere due to the presence of a grating lobe. Therefore, eavesdroppers located away from the intended secure direction can still access freely to the transmitted information. In addition, the profile of this antenna is not low due to height of the monopole.

In this contribution, we reduce the physical profile of the antenna proposed in [16] by eliminating the monopole. We also remove the quadrature condition for exciting the orthogonal  $TM_{21}$  modes suggested in [17] so they can be excited independently. We also add another patch that supports two orthogonal  $TM_{31}$  modes operating at the same frequency as the  $TM_{21}$  modes. As a result, this new design produces DM with low BER in a unique, unambiguous direction in the XY plane if the four available radiation patterns are combined in a prescribed manner.

This document is structured as follows. Section II presents the antenna design and the measurements of reflection coefficient and isolation between antenna ports. In section III, we show the measured radiation patterns for each mode and describe the procedure to generate dynamic DM with the proposed antenna. In section IV, we evaluate experimentally the BER in the XY plane to demonstrate the existence of a single low BER (secure) direction. Finally, in section V, we summarize the conclusions of this work.

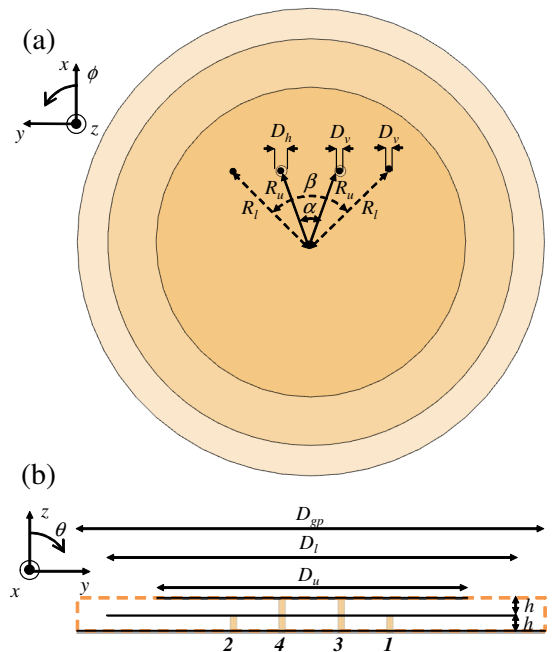


Fig. 1. Scheme of the proposed antenna. Dimensions (in mm) are:  $D_{gp} = 85$ ,  $D_u = 56.4$ ,  $D_l = 74$ ,  $h = 3$ ,  $R_l = 20$ ,  $R_u = 14$ ,  $D_h = 2$ ,  $D_v = 1.3$ . Angles (in degrees) are  $\alpha = 45$ ,  $\beta = 90$ . (a) Upper view. (b) Side view.

Manuscript received May 2020. This work was supported by the Universitat Autònoma de Barcelona, FEDER funds and the Spanish Ministry of Science, Innovation and Universities (RTI2018-096019-B-C33).

J. Parron, E. Cabrera-Hernandez, Pedro de Paco are with the Department of Telecommunications & Systems Engineering, Universitat Autònoma de Barcelona, Catalunya, Spain. Josep.Parron@uab.cat

A. Tennant is with the Department of Electronic and Electrical Engineering at The University of Sheffield, U.K.

Color versions of one or more of the figures in this communication are available online at <http://ieeexplore.ieee.org>.

Digital Object Identifier 10.1109/TAP.2016.xxx

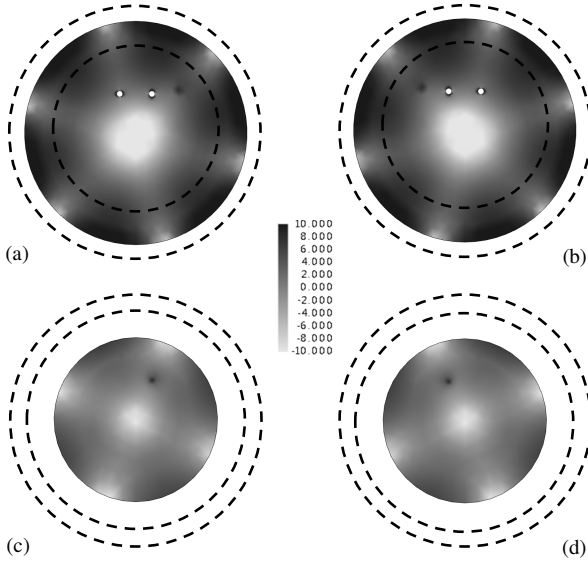


Fig. 2. Simulated current distribution (dBA/m) at 2.435 GHz when one port is fed and the others are loaded with 50  $\Omega$ . (a) Port 1, mode  $TM_{31}$  in lower patch. (b) Port 2, mode  $TM_{31}$  (orthogonal) in lower patch. (c) Port 3, mode  $TM_{21}$  in upper patch. (d) Port 4, mode  $TM_{21}$  (orthogonal) in upper patch.

## II. ANTENNA DESIGN

The proposed multiport antenna consists of two stacked circular microstrip patches that support four radiating modes at the frequency of 2.435 GHz (Fig. 1). The substrate used for both patches is TACONIC TRF 45 ( $\epsilon_r = 4.5$ ,  $\tan\delta = 0.0037$ ) with thickness 3 mm.

The lower patch diameter ( $D_l$ ) was chosen to generate the  $TM_{31}$  mode [18]. This patch is fed through two vias of diameter  $D_v$  that form an angle  $\beta = 90^\circ$  with respect to the disc center in order to excite two orthogonal modes (Fig. 2a and 2b). Theoretically,  $\beta = 30^\circ$  is also an option but, in that case, SMA connectors overlap. The upper patch diameter ( $D_u$ ) was adjusted to obtain the  $TM_{21}$  mode [18] at the same frequency as the  $TM_{31}$  mode. The two orthogonal modes of the upper patch (Fig. 2c and 2d) are fed using two vias of diameter  $D_v$  that pass through the lower patch and form an angle  $\alpha = 45^\circ$  with respect to the disc center. A hole of diameter  $D_h$  was milled in the lower patch to provide isolation between these vias and the lower patch. The relative angular position between the vias that feed each patch was chosen in order to obtain a symmetric design that maximizes isolation among ports whereas the distances  $R_l$  and  $R_u$  were optimized to match the ports to 50  $\Omega$ .

The antenna was fabricated (Fig. 3) using the dimensions that can be found in Fig. 1 and the measured S parameters are presented in Fig. 4. All the ports show optimum matching around 2.435 GHz, however, the measured bandwidth (referred to -10 dB) is lower for modes  $TM_{31}$  (12 MHz) than for modes  $TM_{21}$  (46 MHz). We did not put a particular emphasis in improving this bandwidth since it can be achieved by increasing the thickness of the dielectric substrate [16]. Measured isolation between modes of the same patch is always better than 25 dB and the isolation between modes of different patches is better than 15 dB.

## III. PRINCIPLES FOR DM OPERATION

If we consider an array of  $N$  antennas along the x-axis, the radiation pattern used for the transmitted symbol  $m$  in a given direction  $\phi$  of the XY plane ( $\theta = 90^\circ$ ) can be written as

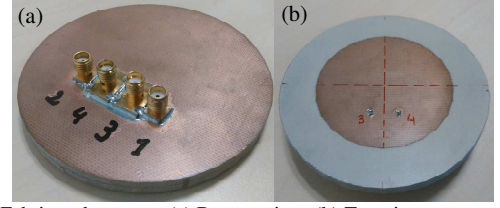


Fig. 3. Fabricated antenna. (a) Bottom view. (b) Top view

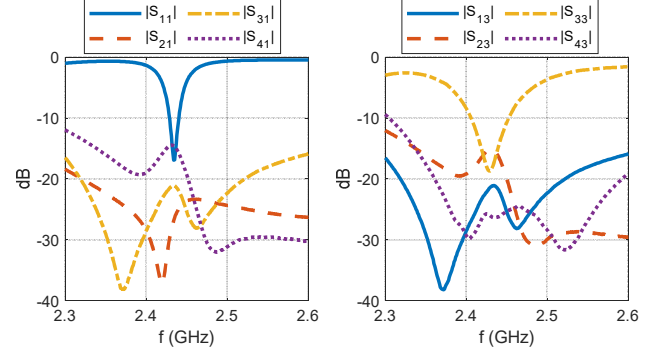


Fig. 4. Measured S parameters. The geometry is symmetric so the S parameters for ports 2 and 4, not shown here for sake of brevity, are almost identical to ports 1 and 3, respectively.

$$S_m(\phi) = \sum_{n=1}^N B_{mn} \cdot AEP_n(\phi) \quad (1)$$

where  $AEP_n(\phi)$  is the active element pattern of antenna  $n$  [19] and  $B_{mn}$  is the weight of antenna  $n$  to transmit symbol  $m$ .

Fig. 5 shows the measured magnitude ( $\theta$  component) of the four AEPs that can be obtained with the proposed antenna design. It must be remarked that orthogonal current distributions generate orthogonal radiation patterns. The measured AEP in the XY plane (magnitude and phase) are plotted in Fig. 6.

To illustrate the process of DM generation, we follow the procedure reported in [12]. First, we calculate the weights  $B_{mn\_conv}$  for conventional modulation: amplitudes are set constant whereas phases are tuned to transmit maximum radiation at the secure direction  $\phi_s$  [12]. Fig. 7 shows as the maximum of radiation can be set arbitrarily in the XY plane with a front to back ratio higher than 10 dB. This is an important improvement with respect to [16] where the front to back ratio was 0 dB. However, the proposed compact antenna also produces two side lobes at approximately  $\phi_s \pm 72^\circ$ , which are only a few dB below the maximum value. High side lobes could compromise the security of a transmission since the signal to noise ratio detected by a potential eavesdropper at those observation angles would be of a similar level to that at the desired recipient. However, DM can help overcome this limitation of the design as described in the following section.

The weights  $B_{mn\_DM}$  that generate DM are computed using the orthogonal vector approach described in [12]. Here, without loss of generality, we consider that the desired secure observation angle is  $\phi_s = 180^\circ$  and the modulation to transmit is QPSK (Fig. 8a). In DM, we increase the total transmitted power by adding a certain amount of orthogonal noise  $W_{mn}$  to the former weights ( $B_{mn\_DM} = B_{mn\_conv} + W_{mn}$ ) so that the transmitted constellation at  $\phi_s$  remains invariant whereas it is scrambled in the other observation angles [12]. The orthogonal noise can be constant for each symbol (static DM) or it can be updated dynamically at the symbol rate (dynamic DM) [20]. The level of security achieved in the communication is related to the extra orthogonal noise power added through the parameter power efficiency [12]

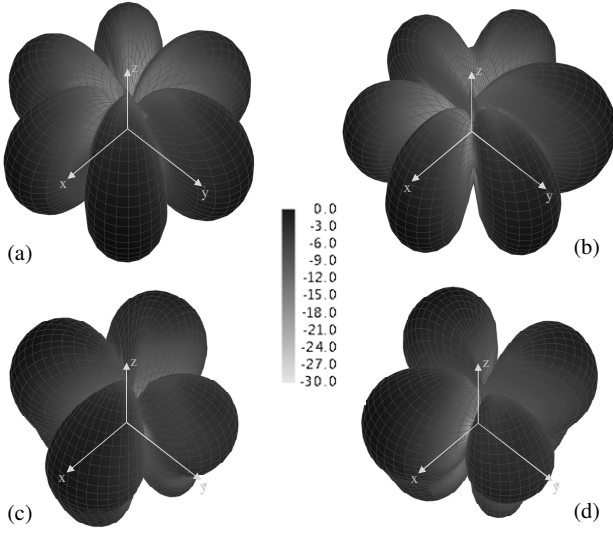


Fig. 5. Measured magnitude (dB) of the AEP ( $\theta$  component) of each mode excited in the antenna at 2.435 GHz. (a) Port 1, mode  $TM_{31}$  in lower patch. (b) Port 2, mode  $TM_{31}$  (orthogonal) in lower patch. (c) Port 3, mode  $TM_{21}$  in upper patch. (d) Port 4, mode  $TM_{21}$  (orthogonal) in upper patch.

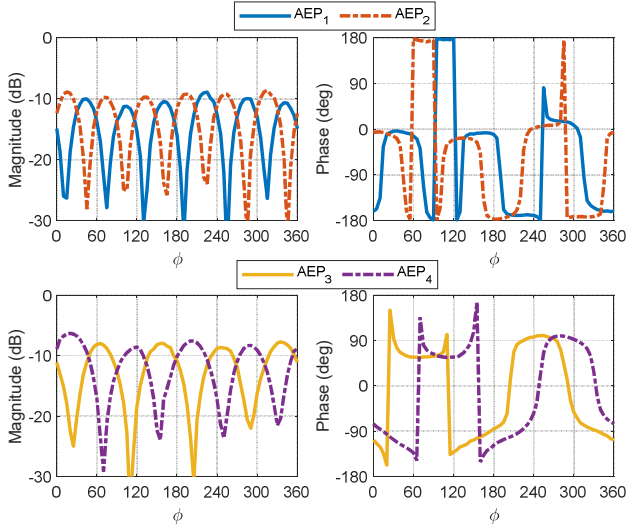


Fig. 6. Measured AEP ( $\theta$  component) in the XY plane

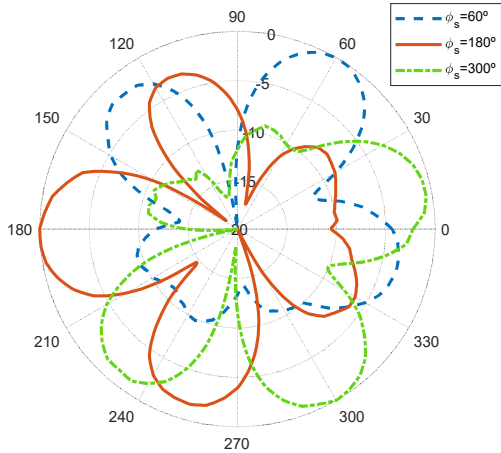


Fig. 7. Normalized radiation patterns (dB) for transmitting a conventional modulation in different secure observation angles  $\phi_s$ .

$$PE_{DM} = \frac{\sum_{m=1}^M \left( \sum_{n=1}^N |B_{mn\_conv}|^2 \right)}{\sum_{m=1}^M \left( \sum_{n=1}^N |B_{mn\_DM}|^2 \right)} \quad (2)$$

where  $M$  is the number of radiation patterns used to generate DM. For a conventional modulation (Fig. 8a),  $PE_{DM}$  is 100% and the improvement of security is related to a decrease in  $PE_{DM}$ .

Indeed, Fig. 8b depicts a set of  $M = 64$  radiation patterns (16 per each QPSK symbol) that can be produced with our antenna to transmit dynamic DM with  $PE_{DM} = 75\%$ . For most observation angles, it is hard to distinguish the shape of the transmitted constellation, however, we still recognize, with a naked eye, noisy QPSK constellations around  $108^\circ$  and  $252^\circ$ . In order to overcome this situation, we further increase the power of orthogonal noise and reduce  $PE_{DM}$  to 50% thus obtaining the radiation patterns of Fig. 8c. Now, we can only recognize, by visual inspection, a QPSK constellation at  $180^\circ$ . Therefore, for a low enough  $PE_{DM}$ , we should be able to obscure the transmitted signal even in the direction of the high side lobes of the conventional radiation pattern and achieve a single secure transmission direction in the XY plane. Note that, in this procedure, radiation patterns are generated randomly without considering the resulting direction of maximum radiation. The performance in terms of  $PE_{DM}$  can be improved if an optimization algorithm is used to select suitable radiation patterns [21].

#### IV. DM PERFORMANCE IN TERMS OF BER

In order to assess the performance of our antenna when it is transmitting dynamic DM in the XY plane, we conducted several measurements with real-time data transmission in a  $5 \times 3 \times 3$  m<sup>3</sup> anechoic chamber. The scheme and photographs of the measurement setup are shown in Fig. 9; distance between transmitting and receiving antennas is 2.5 m. The selected operating frequency was 2.435 GHz and the bit rate 6 Mbps.

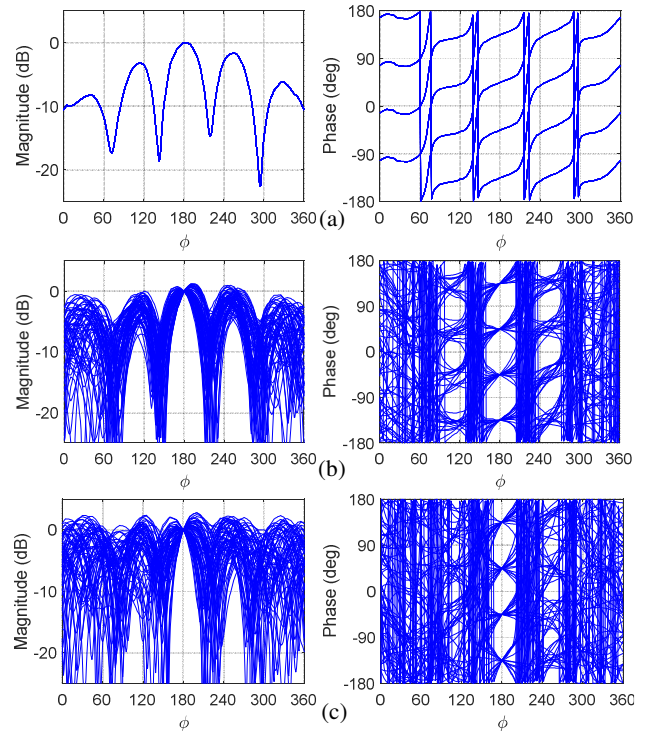


Fig. 8. Magnitude and phase of the generated radiation patterns for transmitting QPSK at  $\phi_s = 180^\circ$  with DM. (a)  $PE_{DM} = 100\%$  (conventional). (b)  $PE_{DM} = 75\%$ . (c)  $PE_{DM} = 50\%$



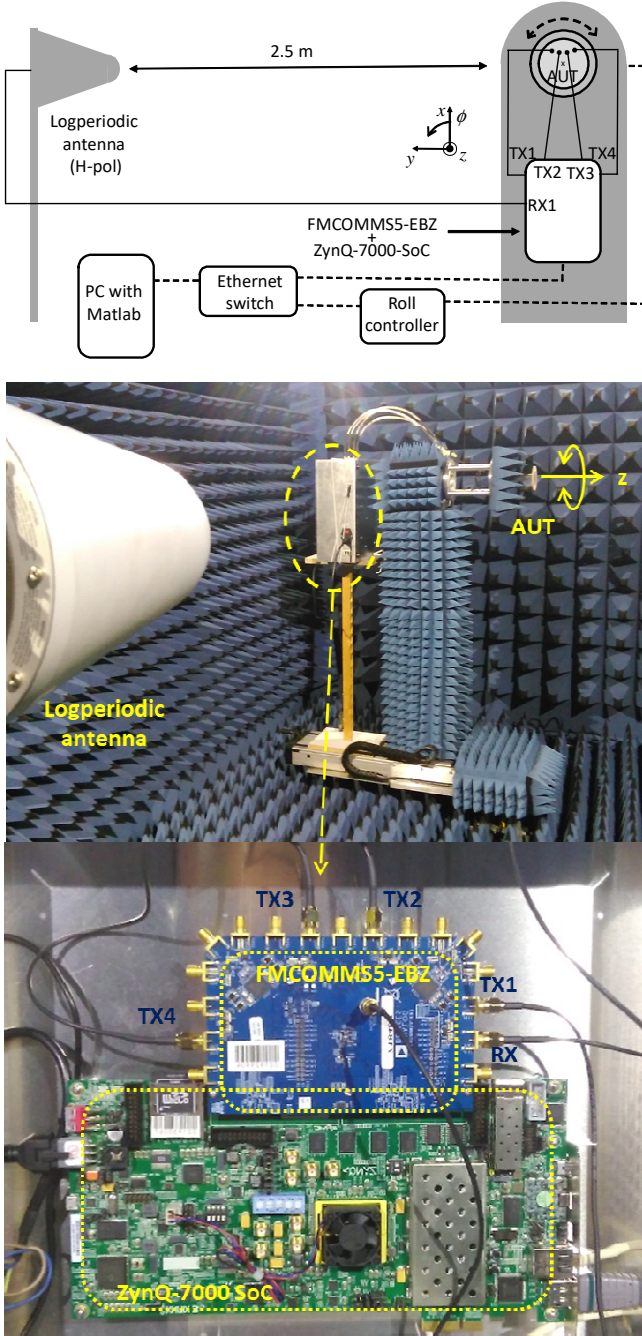


Fig.9. Experimental setup for the measurement of BER in the XY plane when the AUT is transmitting dynamic DM.

The weights  $B_{mn}$  that feed our antenna were previously computed using Matlab and generated in the evaluation board FMCOMMS5-EBZ [22], a FPGA Mezzanine Card (FMC) that is mounted on the ZynQ-7000 SoC ZC706 evaluation kit of Xilinx [23]. The board FMCOMMS5-EBZ contains two AD9361 transceivers, each one of them with two transmitters and two receivers. In our setup (Fig.9), each one of the transmitters was connected to a port of our compact antenna (AUT) whereas one of the board receivers was connected to a log-periodic antenna. Control of transmitted and received signals, as well as the rotation of the AUT, was carried out via Ethernet using Matlab.

The usual metric for evaluating the performance of a DM system is bit-error-rate (BER) [20]; we computed it using the following

assumptions, which are similar to those in [12]:

- QPSK modulation with Gray coding.
- The receiver does not assume a priori any modulation function. Instead, there is a training stage where the receiver computes reference symbols for every observation direction by averaging all the received training symbols. In the transmission stage, the receiver decides which of these reference symbols is received using the minimum Euclidean distance.
- Uniform additive white Gaussian noise (AWGN) in all observation directions. Signal to noise ratio (SNR) will be set to 12 dB for the receiver at the secure direction. Thus, the SNR will change accordingly in the other observation directions. Since the system intrinsic AWGN is low enough to be ignored, artificial AWGN is added onto the received raw data in Matlab.
- Data stream with  $10^6$  transmitted symbols.

In a first experiment, we considered that the desired secure observation angle was  $\phi_s = 180^\circ$ . Fig. 10 displays the simulated and measured BER for different values of  $PE_{DM}$ , both results are in good agreement, in particular around  $\phi_s$ . In the case of  $PE_{DM} = 100\%$ , BER follows the trend of the conventional radiation pattern of Fig 8a. and, consequently, there is only a single angular region in the XY plane with  $BER < 10^{-3}$ . When dynamic DM was introduced (decreasing  $PE_{DM}$ ), we verified that there was a reduction of the beamwidth with  $BER < 10^{-3}$  and the BER in the side lobes decreased, approximately, one order of magnitude.

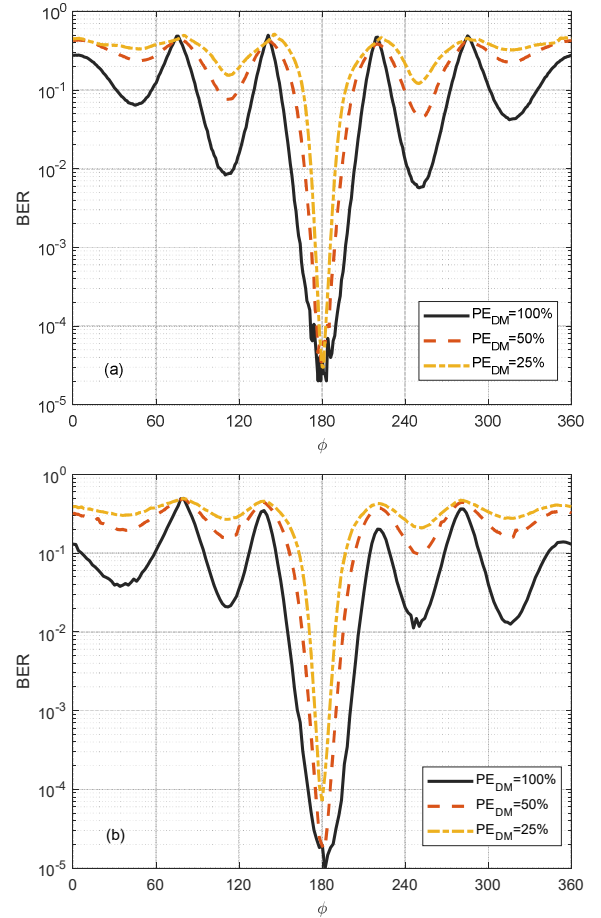


Fig.10. BER angular distribution for different values of  $PE_{DM}$ . AWGN is set to obtain at  $180^\circ$  a SNR of 12 dB. (a) Simulated. (b) Measured.

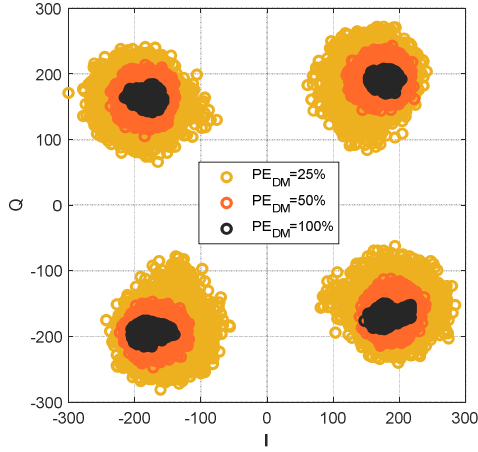
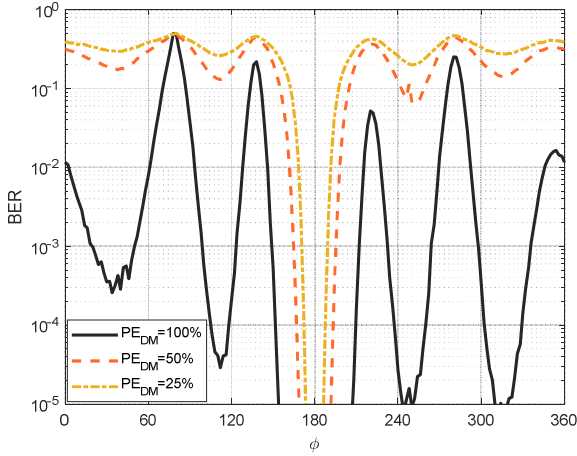


Fig.11. Received constellations at 180° before adding AWGN.


 Fig.12. Measured BER angular distribution for different values of  $PE_{DM}$ . AWGN is set to obtain at 180° a SNR of 18 dB.

In Fig. 10b we can also observe that, at  $\phi_s = 180^\circ$ , there is a slight increase of the measured BER as  $PE_{DM}$  decreases although the added AWGN is the same for the three cases. Fig. 11 depicts the measured constellations in the observation angle before adding AWGN where it can be deduced that the received signal becomes noisier as  $PE_{DM}$  decreases. This aspect was already addressed with simulations in [24], showing that this noise could be eliminated through an accurate calibration (magnitude and phase) of the transmitters return loss. In our case, the board specifications only mention return losses higher than 10 dB and, although they are good enough for a standard application, they can produce an increasingly noisy constellation at  $\phi_s$  as the  $PE_{DM}$  is reduced in order to achieve a narrower secure beam width.

As potential eavesdroppers could have higher signal level than the desired receiver (e.g. because they are closer to the transmit antenna), we carried out a second experiment where the performance of the system was evaluated under an arbitrary improvement of 6 dB in SNR (Fig. 12). If we recall that eavesdroppers also follow the training stage before demodulating, this scenario is very unfavorable from the point of view of security. If we compare Fig. 12 to Fig. 10b, we see, as expected, an important decrease of BER around  $\phi_s$  for all measurements and a slight increase of the beamwidth with  $BER < 10^{-3}$ . Regarding the side lobes, we find four additional angular regions with  $BER < 10^{-3}$  for the conventional modulation ( $PE_{DM} = 100\%$ ). However, in the case of dynamic DM with  $PE_{DM} = 50\%$  there only exists a slight improvement of BER in the main side lobes

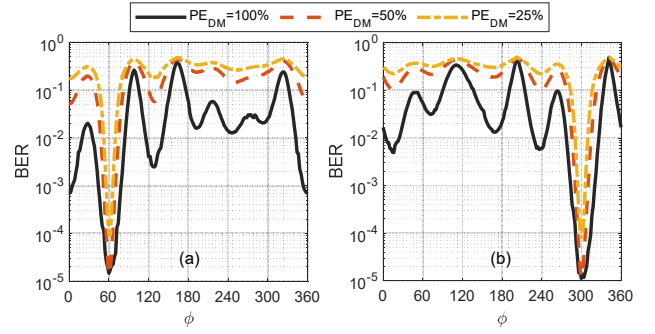

 Fig.13. Measured BER angular distribution for different values of  $PE_{DM}$ . AWGN is set to obtain a SNR of 12 dB in the secure direction. (a)  $\phi_s = 60^\circ$ . (b)  $\phi_s = 300^\circ$ .

TABLE I

 BER MEASUREMENTS FOR DIFFERENT  $PE_{DM}$  VALUES, SNR @  $\phi_s = 12$  DB.

SUMMARY

$PE_{DM} = 100\%$				
$\phi_s$	$\Delta\phi$ BER < $10^{-3}$	BER @ $\phi_s$	BER @ $\phi_s - 72^\circ$	BER @ $\phi_s + 72^\circ$
60°	34°	$1.5 \cdot 10^{-5}$	$7.0 \cdot 10^{-4}$	$2.5 \cdot 10^{-3}$
180°	38°	$1.9 \cdot 10^{-5}$	$2.0 \cdot 10^{-2}$	$1.2 \cdot 10^{-2}$
300°	36°	$1.1 \cdot 10^{-5}$	$5.7 \cdot 10^{-3}$	$5.0 \cdot 10^{-3}$
$PE_{DM} = 50\%$				
$\phi_s$	$\Delta\phi$ BER < $10^{-3}$	BER @ $\phi_s$	BER @ $\phi_s - 72^\circ$	BER @ $\phi_s + 72^\circ$
60°	18°	$1.3 \cdot 10^{-5}$	$5.7 \cdot 10^{-2}$	$6.1 \cdot 10^{-2}$
180°	20°	$2.0 \cdot 10^{-5}$	$1.5 \cdot 10^{-1}$	$1.0 \cdot 10^{-1}$
300°	19°	$1.1 \cdot 10^{-5}$	$1.0 \cdot 10^{-1}$	$1.0 \cdot 10^{-1}$
$PE_{DM} = 25\%$				
$\phi_s$	$\Delta\phi$ BER < $10^{-3}$	BER @ $\phi_s$	BER @ $\phi_s - 72^\circ$	BER @ $\phi_s + 72^\circ$
60°	10°	$9.0 \cdot 10^{-5}$	$1.8 \cdot 10^{-1}$	$2.0 \cdot 10^{-1}$
180°	11°	$7.1 \cdot 10^{-5}$	$2.7 \cdot 10^{-1}$	$2.1 \cdot 10^{-1}$
300°	11°	$7.7 \cdot 10^{-5}$	$2.2 \cdot 10^{-1}$	$2.2 \cdot 10^{-1}$

region and there is not a noticeable change in the case of  $PE_{DM} = 25\%$ . Therefore, we can achieve, with our antenna, a secure transmission in a single angular region of the XY plane no matter how good the eavesdropper SNR is away of this region.

Our last experiment was devoted to verify that a single secure angular region could be set freely in the XY plane (0-360°). Fig. 13 shows the measured BER for different values of  $PE_{DM}$  and  $\phi_s$ .

For sake of comparison, Table I summarizes the main results extracted from Fig. 10 and Fig. 13. Firstly, we can see that, for a given  $PE_{DM}$ , the same beamwidth with  $BER < 10^{-3}$  is achieved around the desired observation angle  $\phi_s$ . Secondly, we noticed that, for  $PE_{DM} = 50\%$ , the BER at the side lobes is, at least, one order of magnitude higher than the conventional modulation ( $PE_{DM} = 100\%$ ). Finally, we want to point out that, again, for  $PE_{DM} = 25\%$ , the BER at the side lobes is of the order of 0.2 and it does not change with the secure observation angle.

## V. CONCLUSIONS

In this contribution, we have presented the design of a multipoint compact stacked patch antenna (diameter  $0.7\lambda$ ) that radiates four different modes at the same frequency. Measured AEPs show variations in magnitude and phase that make this antenna a suitable candidate for generating dynamic direction dependent antenna modulation. The compact stacked patch antenna can provide equivalent performance to a conventional 4 element array with a spacing of  $\lambda/2$ , but with significantly reduced size.

Our design improves the previous work in [16] in two main aspects. Firstly, the removal of the monopole results in a low profile antenna (thickness  $0.05\lambda$ ). Secondly, the combination of the four radiating modes (instead of two) allows the generation of a radiation pattern with a front to back ratio of at least 10 dB and  $360^\circ$  steering.

The performance of a prototype stacked patch antenna has been investigated experimentally using the evaluation board FMCOMMS5-EBZ. In particular, the measured performance of this antenna when used to generate dynamic DM in terms of BER and  $PE_{DM}$  has been presented. Checks were made to verify that the minimum BER at the desired observation angle degrades for low  $PE_{DM}$ . It has also been verified that for  $PE_{DM} = 50\%$  it is possible to obtain a single low BER angular region for any observation angle in the XY plane. To the best of authors' knowledge, this is the first time this behavior is reported and it improves significantly the performance of the DM system in [17]. Finally, we observed that, for  $PE_{DM} = 25\%$ , the BER at the side lobes remains almost invariant with the observation angle and the SNR. Therefore, dynamic DM can compensate the threat to security generated by the high side lobes in the radiation pattern of our antenna.

From the previous results, it could be concluded that the required  $PE_{DM}$  for a single secure angle is too low to be acceptable in some practical applications where the transmitter power is limited. However, this is a quite a remarkable result if we consider that the algorithm that generates the DM weights does not use any optimization technique to improve the results. Additionally, it must be noted that the measurement procedure assumes a worst-case scenario in which the eavesdroppers are pre-trained. Therefore, the proposed scenario is very unfavorable from the point of view of security and a much better performance can be expected in a practical scenario.

#### REFERENCES

- [1] A. Mukherjee, S. Ali A. Fakoorian, J. Huang, A. Lee Swindlehurst, "Principles of Physical Layer Security in Multiuser Wireless Networks: A Survey," *IEEE Commun. Surveys Tuts.*, vol. 16, no. 3, pp. 1550-1573, 2014.
- [2] Y. Ding, V. Fusco, "Directional Modulation Enabled Physical-layer Wireless Security," in *Trusted Communications with Physical Layer Security for 5G and Beyond*, IET, 2018.
- [3] A. Babakhani, D. B. Rutledge, and A. Hajimiri, "Near-field direct antenna modulation," *IEEE Microw. Mag.*, vol. 10, no. 1, pp. 36-46, Feb. 2009.
- [4] N. Valliappan, A. Lozano, and R. W. Heath, "Antenna subset modulation for secure millimeter-wave wireless communication," *IEEE Trans. on Commun.*, vol. 61, no. 8, pp. 3231-3245, 2013.
- [5] Q. Zhu, S. Yang, R. Yao, and Z. Nie, "Directional modulation based on 4-D antenna arrays," *IEEE Trans. Antennas Propag.*, vol. 62, no. 2, pp. 621-628, 2014.
- [6] C. Sun, S. Yang, Y. Chen, J. Guo, S. Qu, and J. Hu, "4-D retrodirective antenna arrays for secure communication based on improved directional modulation," *IEEE Trans. Antennas Propag.*, vol. 66, no. 11, pp. 5926-5933, 2018.
- [7] T. Hong, M.-Z. Song, and Y. Liu, "Dual-beam directional modulation technique for physical-layer secure communication," *IEEE Antennas Wireless Propag. Lett.*, vol. 10, pp. 1417-1420, 2011.
- [8] M. P. Daly and J. T. Bernhard, "Directional modulation technique for phased arrays," *IEEE Trans. Antennas Propag.*, vol. 57, no. 9, pp. 2633-2640, 2009.
- [9] M. P. Daly, E. L. Daly, and J. T. Bernhard, "Demonstration of directional modulation using a phased array," *IEEE Trans. Antennas Propag.*, vol. 58, no. 5, pp. 1545-1550, May 2010.
- [10] H. Shi, A. Tennant, "Simultaneous Multichannel Spatially Directive Data Transmission Using Direct Antenna Modulation," *IEEE Trans. Antennas Propag.*, vol. 62, no. 1, pp. 403-410, 2014.
- [11] S. Mufti, J. Parrón, A. Tennant, "Hardware implementation of directional modulation system with a 2 element antenna array," in *11th European Conference on Antennas and Propagation (EUCAP)*, Paris (France), pp. 3239-3242, 2017.
- [12] Y. Ding and V. Fusco, "A vector approach for the analysis and synthesis of directional modulation transmitters," *IEEE Trans. Antennas Propag.*, vol. 62, no. 1, pp. 361-370, 2014.
- [13] Y. Ding and V. Fusco, "A review of directional modulation technology," *International Journal of Microwave and Wireless Technologies*, vol. 8, no. 7, pp. 981-993, 2016.
- [14] Y. Ding and V. Fusco, "A synthesis-free directional modulation transmitter using retrodirective array," *IEEE J. Sel. Topics Signal Process.*, vol. 11, no. 2, pp. 428-441, Mar. 2017.
- [15] Y. Ding, Y. Zhang, and V. Fusco, "Fourier Rotman Lens Enabled Directional Modulation Transmitter," *International Journal of Antennas and Propagation*, vol. 2015, Article ID 285986, 13 pages, 2015.
- [16] A. Narbudowicz, M. J. Ammann, D. Heberling, "Switchless Reconfigurable Antenna with  $360^\circ$  Steering," *IEEE Antennas and Wireless Propag. Lett.*, vol. 15, pp. 1689-1692, 2016.
- [17] A. Narbudowicz, M. J. Ammann, D. Heberling, "Directional Modulation for Compact Devices," *IEEE Antennas and Wireless Propag. Lett.*, vol. 15, pp. 1689-1692, pp. 2094-2097, 2017.
- [18] R. Garg, P. Bhartia, I. Bahl, A. Ittipiboon, "Circular Disk and Ring Antennas," in *Microstrip Antenna Design Handbook*, Artech House, 2001.
- [19] D. M. Pozar, "The active element pattern," *IEEE Trans. Antennas Propag.*, vol. 42, no. 8, pp. 1176-1178, 1994.
- [20] Y. Ding and V. F. Fusco, "Establishing metrics for assessing the performance of directional modulation systems," *IEEE Trans. Antennas Propag.*, vol. 62, no. 5, pp. 2745-2755, 2014.
- [21] Y. Ding and V. F. Fusco, "Constraining directional modulation transmitter radiation patterns," *IET Microw. Antennas Propag.*, vol. 8, no. 15, pp. 1408-1415, 2014.
- [22] AD-FMCOMMS5-EBZ evaluation board [Online]. Available: <https://www.analog.com/en/design-center/evaluation-hardware-and-software/evaluation-boards-kits/eval-ad-fmcomms5-ebz.html>.
- [23] ZynQ-7000 SoC evaluation kit [Online]. Available: <https://www.xilinx.com/products/boards-and-kits/ek-z7-zc706-g.html>.
- [24] E. A. Cabrera-Hernández, J. Parrón and A. Tennant, "On the Implementation of a Dynamic Direction Modulation System with Vector Modulators," *International Journal of Antennas and Propagation*, vol. 2019, Article ID 9784252, 13 pages, 2019.